Synthesis of Monodispersed Red Emitting LiAl5O8:Fe3+ Nanophosphors

Article *in* Science of Advanced Materials · May 2012

DOI: 10.1166/sam.2012.1325

CITATIONS
10

READS
587

5 authors, including:

Abhijit P. Jadhav
Pusan National University
21 PUBLICATIONS **413** CITATIONS

SEE PROFILE

Umapada Pal
Benemérita Universidad Autónoma de Puebla
255 PUBLICATIONS **9,274** CITATIONS

SEE PROFILE

Byung Kim
Pusan National University
520 PUBLICATIONS **15,927** CITATIONS

SEE PROFILE

AMERICAN SCIENTIFIC PUBLISHERS

Science of Advanced Materials
Vol. 4, pp. 597–603, 2012
(www.aspbs.com/sam)

Synthesis of Monodispersed Red Emitting $LiAl_5O_8:Fe^{3+}$ Nanophosphors

Abhijit P. Jadhav[1], Amol Pawar[1], U. Pal[2], Byung Kyu Kim[3], and Young Soo Kang[1,*]

[1]*Department of Chemistry, Sogang University, Seoul, 121 742, Republic of Korea*
[2]*Instituto de Fisica Benemerita, Universidad Autonoma de Puebla, Apodo. Postal J-48, Puebla, Pue 72570, Mexico*
[3]*Department of Polymer Science and Engineering, Pusan National University, Pusan, 609-735, Republic of Korea*

ABSTRACT

Efficient wavelength converting nanophosphors are of high demand for their applications in energy conversion devices. We report on the synthesis of well dispersed $LiAl_5O_8:Fe^{3+}$ nanoparticles of homogeneous size and different morphologies by sol–gel method suitable for efficient wavelength converting devices. Nanoparticles of phase pure Fe^{3+} doped $LiAl_5O_8$ with different shapes and sizes were obtained by varying the pH of the solution in the range of 3–11. X-ray diffraction, transmission electron microscopy and X-ray photoelectron spectroscopy were used to analyze the structure, morphology and composition of the nanoparticles. Incorporation of Fe^{3+} ions in the $LiAl_5O_8$ host lattice has been studied using X-ray photoelectron spectroscopy and electron spin resonance spectroscopy. Emission behavior of the nanophosphors has been studied at room temperature using photoluminescence spectroscopy.

KEYWORDS: Lithium Aluminate, Nanophosphors, X-Ray Electron Spectroscopy, Photoluminescence.

1. INTRODUCTION

While solar radiation is the biggest source of energy in the earth, photosynthesis process is the basic source of plant growth. The pigments like chlorophyll and carotenoid have the ability to convert solar energy to chemical energy.[1] It has been observed that photosynthesis process in plants is faster and efficient under the blue and red lights of the solar spectrum.[2] So, for a better utilization of solar energy in photosynthesis process, conversion of UV light of the solar spectrum into visible and near infra-red is essential. For this purpose, development of down-converting phosphors, which can convert the high energy radiation of the solar radiation to lower energy range, is very important. Wavelength converting red emitting phosphors are convenient materials for artificial illumination in polyhouses for plant growth.[3] Down converting nanophosphors which can convert high energy of the solar radiation to visible or near infrared can be used to prepare polyolefin composite films and applied for plant growth. Though the use of inorganic phosphors in this area is not very common, recently several nanophosphors like $BaMg_2Al_{10}O_{17}:Eu$, $Y_2O_3:Eu^{3+}$, $CaAl_4O_7:Tb^{3+}$, $CaAl_4O_7:Ce^{3+}$ have been tested for this purpose and the obtained results were quite encouraging.[4–6] In fact, incorporation of inorganic nano-phase materials in polymer matrix is advantageous over the organic fillers, as they do not react with the polymer matrix, maintaining the durability of the composite films. On the other hand, incorporation of inorganic nanoparticles in polymer matrix makes a little impact on the mechanical properties of the polymer film. Such inorganic-nanoparticle incorporated polymeric composite films are environmental friendly, and have great potential for applications in energy conversion processes. As has been reported by Purves et al., the well-known pigment chlorophyll absorbs solar light from violet to blue and from reddish orange to red wavelength regions.[1] Therefore, development of efficient down-converting nanophosphors which can emit in these regions is of immense technological interest.

In this article, we present the synthesis and emission behaviors of Fe^{3+} doped $LiAl_5O_8$ nanophosphors which have the potential for greenhouse applications. Though the undoped $LiAl_5O_8$ has no direct technological application, $LiAl_5O_8:Fe^{3+}$ is one of the prominent phosphor materials, capable of converting UV-visible portion of the solar radiation to red.

Synthesis of $LiAl_5O_8$ doped with different transition metals such as Cr^{3+},[7] Fe^{3+},[8] Mn^{2+},[9] Co^{2+} [10] and rare earths like Eu^{3+} [11] have been reported by several research groups. Very often, the combustion method has been utilized for this purpose, where metallic precursors were

*Author to whom correspondence should be addressed.
Email: yskang@sogang.ac.kr
Received: 30 April 2011
Revised/Accepted: 3 July 2011

ARTICLE

mixed and heated at high temperature.[12] Apart from combustion, other physical methods like self-flux synthesis[13] and vapor phase transport process[14] have also been utilized to synthesize $LiAl_5O_8$ nanostructures recently. Most of these physical methods have limitations as they need lengthy mechanical mixing, high temperature annealing or lengthy heat treatments. Moreover, the samples obtained through physical techniques are not in phase pure form, as there is no control over the formation of other phases during reaction.[13] Due to the formation of undesired secondary phases the energy levels and electronic transitions of dopant atoms get changed and this may affect the optical properties of the phosphor material.[15] Another disadvantage of the physical methods is that there is no control over growth of particles, i.e., control of particle size, crystallinity and morphology. There exist several reports on the synthesis of $LiAl_5O_8$ nanostructures by wet chemical methods such as sol–gel,[16] hydrothermal and precipitation.[8] Most of these wet chemical methods produce phase pure $LiAl_5O_8$. However, reports on the synthesis of $LiAl_5O_8$ by wet chemical methods with controlled size, shape and crystallinity are limited.[10] While the optical properties of rare-earth doped metal oxides depend mainly on the dopant concentration, it has also been observed that an increase in particle size may lead to a redshift in emission wavelength.[17]

In this article we report on the synthesis of efficient wavelength converting $LiAl_5O_8$:Fe^{3+} nanoparticles of controlled size and shape by varying the reaction conditions in a wet chemical technique. The nanoparticles are highly crystalline and monodispersed. Different morphologies of $LiAl_5O_8$:Fe^{3+} nanoparticles could be obtained by controlling the pH of the reaction solution. Growth mechanism and emission behavior of the nanoparticles have been discussed.

2. EXPERIMENTAL DETAILS

2.1. Materials

Lithium hydroxide monohydrate ($LiOH \cdot H_2O$, 98% Aldrich), aluminum chloride ($AlCl_3$, 99.99% Aldrich), iron chloride hexahydrate ($FeCl_3 \cdot 6H_2O$, Acros Organics), tartaric acid ($C_4H_6O_6$, extra pure, Junsei Chemical Co. Ltd.) and sodium hydroxide (NaOH, extra pure, Samchun Chemical Co. Ltd.) were used as received without further purification.

2.2. Synthesis

Synthesis of Fe^{3+} doped $LiAl_5O_8$ was carried out by sol–gel method. First the precursors such as lithium hydroxide monohydrate (0.004 mol), aluminum chloride (0.02 mol) and iron chloride hexahydrate (0.0005 mol) were dissolved in 100 mL of deionized (DI) water in a round bottom flask. Then a 50 mL of aqueous tartaric acid solution (0.005 mol) was added slowly to the earlier mixture as a complex forming agent. The mixture was then stirred at room temperature for 1 h using magnetic stirrer. The pH of the reaction mixture was adjusted either to 3, 5, 7, 9 or 11, by adding different amounts of a 1.0 M NaOH solution. The reaction mixture was then heated to 80 °C and maintained at this temperature for 4 h, under continuous magnetic stirring. The orange colored sol finally converted into thick gel which was dried at 120 °C for 6 h in air. The obtained powders were air annealed at 1200 °C for 6 h using a muffle furnace.

2.3. Characterizations

X-ray diffraction (XRD) patterns of the as-prepared and annealed powder samples were recorded using the Cu Kα radiation ($\lambda = 1.54056$ Å) of a Rigaku X-ray diffractometer operating at 40 kV and 150 mA, at a scanning rate of 0.02° per second in the range of $2\theta = 10 - 90°$. Surface composition and chemical state of the constituting elements of the phosphor particles were evaluated by a Thermo VG Scientific (England), Multitab 2000 X-ray photoelectron spectrometer (XPS). Size and shape of the synthesized particles were examined with JEOL JEM 2100F transmission electron microscope (TEM) operating at 200 kV. For TEM observations, the samples were prepared by placing a drop of cyclohexane dispersed colloids over the carbon coated microscopic grids (300 mesh size) and subsequent drying under infra-red illumination. Electron spin resonance (ESR) spectra of the nanoparticles were recorded at room temperature on a JEOL (Japan), JES PX 2300 FT-ESR magnetometer. Room temperature photoluminescence (PL) emission spectra of the powder samples were measured with a Hitachi F-7000 fluorescence spectrophotometer, using the 200 nm excitation of a Xenon lamp.

3. RESULTS AND DISCUSSION

For the effective wavelength conversion, the phosphor materials should be in nanometer regime and have homogeneous distribution in the matrix. Higher efficiency of wavelength conversion is expected for the phosphor nanoparticles of uniform size distribution. For obtaining uniform particle size, a careful control of reaction parameters during sol–gel process is necessary. The size of the colloidal particles and their aggregation depend on several factors such as pH, composition of the reaction mixture, and reaction temperature.[18] In sol–gel synthesis of $LiAl_5O_8$:Fe^{3+} nanoparticle, pH of the reaction mixture plays significant roles in controlling their growth and emission behaviors. Growth mechanisms of nanoparticles in sol–gel reaction have been proposed by several researchers.[19–24]

Figure 1 presents the typical TEM images of $LiAl_5O_8$:Fe^{3+} samples prepared at different pH values of

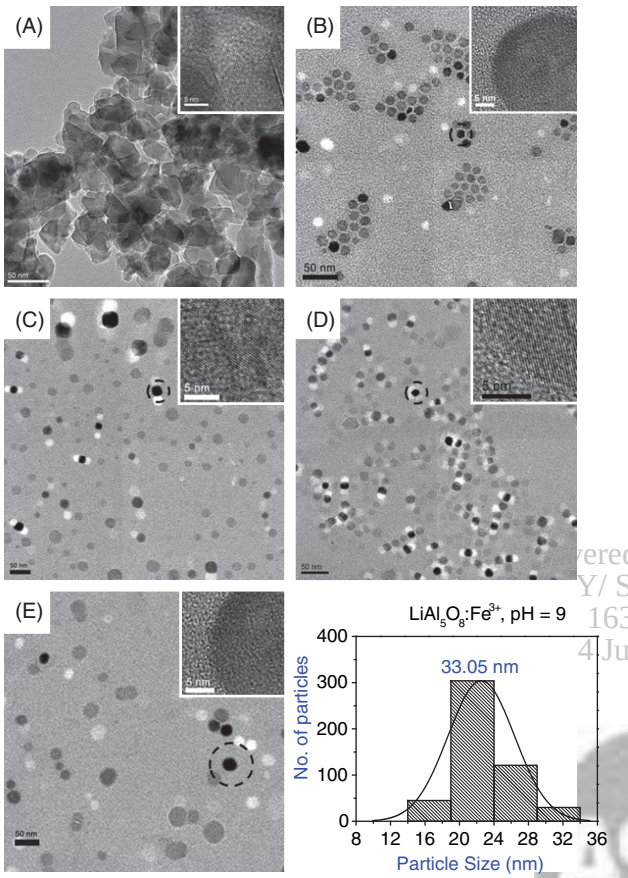

Fig. 1. Typical TEM images of $LiAl_5O_8:Fe^{3+}$ samples synthesized at: (A) pH = 3, (B) pH = 5, (C) pH = 7, (D) pH = 9 and (E) pH = 11. Corresponding high resolution images are shown as insets. Particle size distribution of $LiAl_5O_8:Fe^{3+}$ synthesized at pH = 9 is also presented. All the samples were annealed at 1200 °C for 6 h in air.

the reaction mixture. Formation of nanometer size particles of well-defined shapes with narrow size distribution and high crystallinity can be observed from the respective TEM images and their high resolution images presented as insets. The average particle size increased from 20 nm to about 37 nm on increasing the pH of the reaction medium. At pH = 3, the highly acidic reaction medium produced agglomerated crystalline nanoparticles of arbitrary shapes, with relatively broader size distribution (Fig. 1(A)). On increasing the pH of the solution to 5, more dispersed nanoparticles with larger size and square shape are obtained (Fig. 1(B)). When the pH of the reaction medium was increased to 7 or 9, even larger nanoparticles of quasi-square shape were obtained (Figs. 1(C and D), respectively). Further increase in pH of the reaction medium to 11 produced well dispersed spherical shaped nanoparticles of larger sizes (Fig. 1(E)). Homogeneity of the produced nanoparticles can be perceived from the size distribution histogram of the sample prepared at pH = 9, as shown in Figure 1. Usually in the case of ceramic oxides, synthesis of material in nanometer regime is difficult due to application of high temperature annealing process. Pan et al.[10] could obtain Co doped $LiAl_5O_8$ nanoparticles of 20–30 nm and 40–50 nm diameters through sol–gel technique by annealing their samples at 700 °C and 900 °C, respectively. Even though their nanoparticles were small enough, the particles were aggregated and of irregular shapes. We carefully controlled the solution pH to obtain small nanoparticles of uniform size distribution, even after annealing at 1200 °C for 6 h. In general, an increase in the pH value of the reaction medium enhanced particle dispersion and produced nanoparticles of larger average sizes (Fig. 2).

The formation process of the nanoparticles, their size and morphology evolutions at different pH values of the reaction mixture are schematically presented in Figure 3. In the case of pH = 3, the rate of hydrolysis depends primarily on the concentration of hydrogen ions $[H^+]$. The hydrolysis and condensation process at low pH condition are relatively controlled and selective, which helps to form linear chains of metal and oxygen.[20, 22] During the polymerization process in sol–gel reaction, the smaller metal-oxygen chains get hydrolyzed prior to the longer chains. In longer metal-oxygen chains the rate of hydrolysis is greater, which helps to produce linear chains.[23] The less cross-linked structure helps to produce nanoparticles of very small size. The attractive and repulsive forces acting on the nanoparticles tend to form their agglomerated structures. $LiAl_5O_8:Fe^{3+}$ synthesized at pH = 3 also shows agglomerated structures with particle size varying in between 20 and 40 nm. Initially the rate of hydrolysis depends on the small amount of $[H^+]$ present in the reaction medium, which helps to produce linear chains. As the amount of hydroxyl ion species increases with increase in pH of the solution, the rate of the hydrolysis and condensation depends on [OH] ions. During gel formation process,

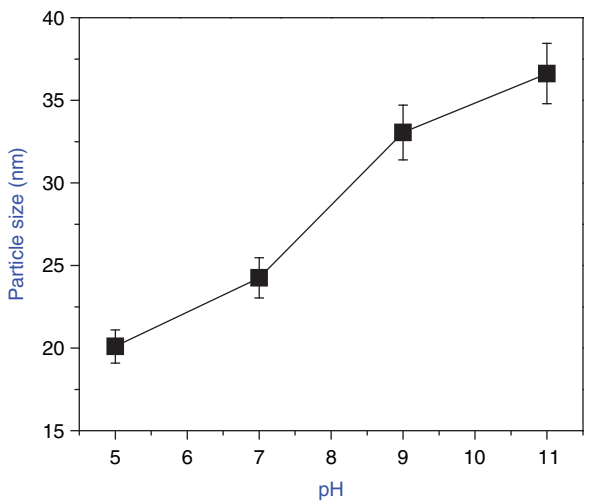

Fig. 2. Variation of particle size and their size dispersion with the variation of the pH value of the reaction mixture in sol–gel process. The error bars correspond to the standard deviations obtained from the Gaussian fits to the size distribution histograms.

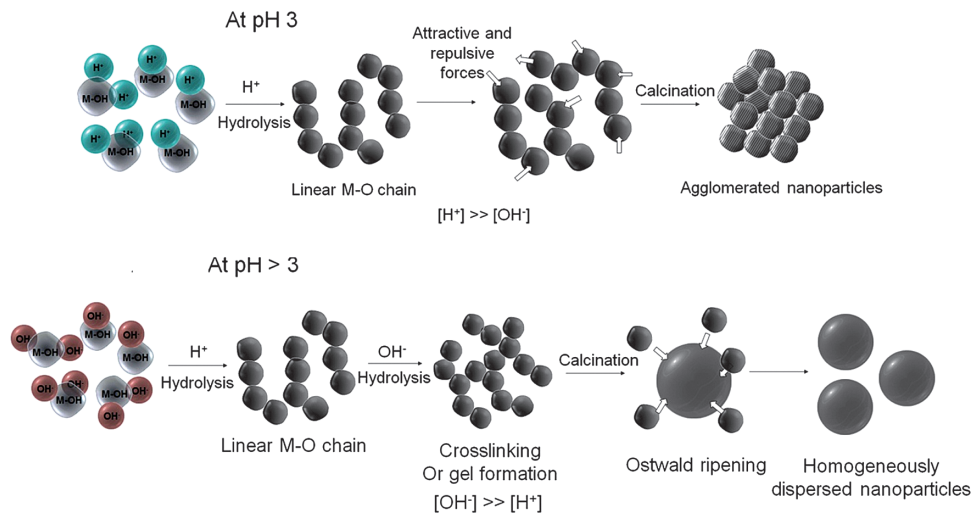

Fig. 3. Schematic presentation of formation process and morphology evolution of $LiAl_5O_8:Fe^{3+}$ nanoparticles in sol–gel process at different pH values.

the higher amount of hydroxyl ions helps to produce cross-linked structures between linear chains as the probability of intermolecular reaction is higher than intramolecular reaction.[25] The processes like hydrolysis and condensation at higher pH values are less controlled and selective, which lead to higher branching and larger interconnected particles.[26] During gel formation, the growth of nanoparticles takes place by Ostwald ripening process, which helps to produce larger nanoparticles as observed in the case of pH values 5–11.

To support the TEM images shown in Figure 1, we measured XRD patterns of the $LiAl_5O_8:Fe^{3+}$ nanoparticles synthesized at different pH values and annealed at 1200 °C for 6 h. Diffraction patterns of the nanoparticles are shown in Figure 4. All the samples revealed well resolved diffraction peaks matching well with the standard diffraction pattern of $LiAl_5O_8$ (JCPDS No. 71-1736). No additional peak related to iron or its oxide was observed in the XRD pattern of the nanoparticles, indicating their phase purity. The average lattice constant evaluated for the samples using the relation $d^2 = a^2/(h^2 + k^2 + l^2)$ was $a =$ 7.9078 Å, which is in good agreement with the standard value of ordered phase $LiAl_5O_8$ ($a = 7.9080$ Å, JCPDS No. 71-1736). Although the variation of pH of the reaction mixture did not generate any other phase rather than $LiAl_5O_8$, the intensity of the (311) peak of the samples reduced drastically when the pH of the reaction mixture was 7 or higher. The result indicates the growth of the nanostructures along [311] direction is preferred probably in acidic reaction medium.

To detect the paramagnetic centers and their surrounding environments in the nanophosphors, electron spin resonance (ESR) spectra of the samples were recorded at room temperature. Figure 5 shows the room temperature ESR spectra of $LiAl_5O_8:Fe^{3+}$ nanophosphors synthesized at different pH values. All the samples revealed single resonance absorption peak. Fe ions with their 3d electronic configuration and $S = 5/2$ should present five line spectra corresponds to $5/2 \leftrightarrow 3/2$, $3/2 \leftrightarrow 1/2$, $1/2 \leftrightarrow -1/2$, $-1/2 \leftrightarrow -3/2$ and $-3/2 \leftrightarrow -5/2$ transitions. Electron spin magnetic moment is associated with electron spin rotation around its own axis. The g factor of a paramagnetic sample is a unit less quantity which depends on the interaction of electron with the total angular momentum, orbital angular momentum and spin angular momentum. The g-value for $LiAl_5O_8:Fe^{3+}$ samples synthesized at pH = 3, 5, 7, 9 and 11 were 1.9986, 2.0014, 1.9848, 2.0011 and 2.0015, respectively. Boesman[27] and Kedzie[28] have observed that when Fe^{3+} occupies octahedral position in $LiAl_5O_8:Fe^{3+}$, the g-value comes around 2.0. Table I shows the line-width of the ESR signal of $LiAl_5O_8:Fe^{3+}$

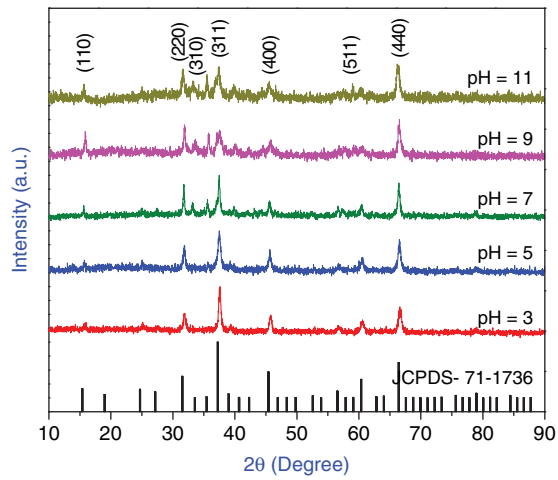

Fig. 4. Comparative XRD patterns of the $LiAl_5O_8:Fe3^{+}$ samples synthesized at different pH values. All the samples were calcinied at 1200 °C for 6 h in air.

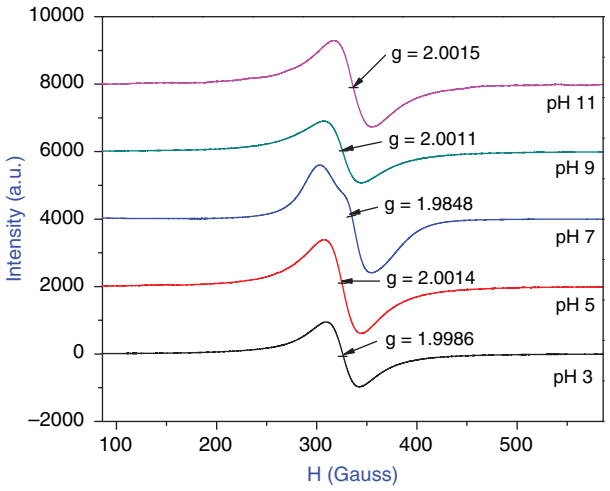

Fig. 5. Room temperature X-band ESR absorption spectra of the $LiAl_5O_8:Fe^{3+}$ nanoparticles synthesized at various pH values.

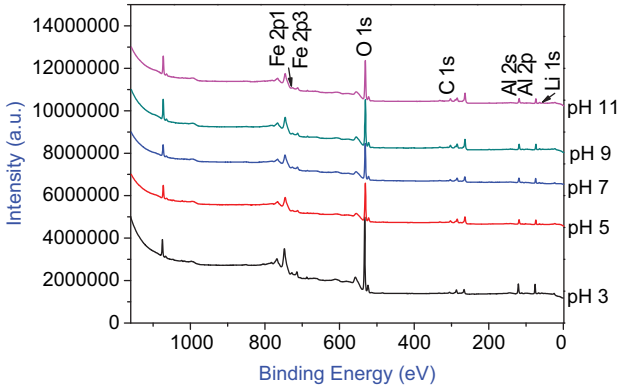

Fig. 6. XPS survey spectra of $LiAl_5O_8:Fe^{3+}$ nanoparticles synthesized at various pH values.

nanophosphors synthesized at different pH values. The line width of the ESR spectrum depends on the interaction between magnetic moment of an electron with surrounding nuclei and their electrons. The line-width increases up to pH = 7 and then decreases for pH = 9 and pH = 11. The broader ESR signal for the sample prepared at pH = 7 is probably due to its higher lattice disorder.[29]

To identify the composition and oxidation state of the constituting elements of the $LiAl_5O_8:Fe^{3+}$, the nanophosphors were analyzed by XPS. Comparative XPS survey spectra of the nanophosphors synthesized at different pH values of the reaction mixture are shown in Figure 6. All the spectra were corrected considering the position of the C1s peak at 284.6 eV as standard. The purpose of XPS analysis was also to get an idea of dopant concentration in $LiAl_5O_8$ at various pH values. Photoelectron spectra of all the samples revealed emission peaks corresponding to Li, Al, O and Fe. XPS surface composition of the samples synthesized at different pH values are presented in Table II. As can be noted in the Table II, though all the samples were prepared at same nominal concentration of iron, the atomic percent of Fe varied with the variation of pH. While the estimated content of Fe in the final product was maximum for the sample synthesized at pH = 3 (1.13 Atom%), the content of Fe was found minimum for the sample synthesized at pH = 5 (0.76 Atom%).

Normally the doping concentration in metal oxide nanostructures depends largely upon the rate of hydrolysis process during sol–gel reaction. The precursor $FeCl_3 \cdot 6H_2O$ dissociates in aqueous solvent to form hexa-aquo ion $[Fe(H_2O)_6^{3+}]$. The electropositive cation induces the H_2O ligands to act as acids and at lower pH value, and the deprotonation of these ligands takes place in stepwise manner.[30] Complete hydrolysis corresponds to the formation of Fe^{III} oxide. The rate of hydrolysis strongly depends upon pH of the medium. As observed in the emission spectra for the activator ion Fe^{3+} in 2p region (Fig. 7), the intensity of the 711.44 eV peak is maximum for the sample prepared at pH = 3. Thus it was clear that, at pH = 3, number of iron hydroxide species in this sample is greater, and hence the amount of iron dopant incorporated into the $LiAl_5O_8$ lattice is higher than the samples prepared at higher pH values. The Fe 2p emission band splits into two sub-bands associated to $Fe2p_{3/2}$ and $Fe2p_{1/2}$ emissions. Iron present in $LiAl_5O_8$ remained bonded with oxygen and aluminum. For the samples prepared at pH values 3, 5, 9 and 11, the peak position of iron represents Fe in Fe(OH)O (iron (III) hydroxide oxide)[31] state appeared at about 711.44, 711.81, 711.61 and 711.86 eV, respectively. The sample synthesized at pH = 7 shows mild red-shift of 0.49 eV from the binding energy value of Fe in Fe(OH)O i.e., 711.8 eV.

Figure 8 shows the schematic presentation of the energy levels in $LiAl_5O_8:Fe^{3+}$ for the down conversion of Fe^{3+} under 453 nm excitation. Fe^{3+} in its excited state shows $3d^5$ electronic configuration. As 'd' subshell of Fe is half

Table I. Line width of ESR signal of $LiAl_5O_8:Fe^{3+}$ synthesized at different pH values. The ESR measurement was carried out at room temperature.

$LiAl_5O_8:Fe^{3+}$ (pH)	Line width (Gauss)
3	334.45
5	370.51
7	518.84
9	368.07
11	378.45

Table II. Elemental composition (in atom %) of the $LiAl_5O_8:Eu^{3+}$ nanoparticles synthesized at different pH values of the reaction mixture.

$LiAl_5O_8:Fe^{3+}$	O (atom %)	Al (atom %)	Li (atom %)	Fe (atom %)
pH 3	48.15	26.81	23.91	1.13
pH 5	47.57	24.96	26.71	0.76
pH 7	41.88	25.79	31.34	0.98
pH 9	48.94	24.20	26.00	0.86
pH 11	48.27	23.66	27.16	0.91

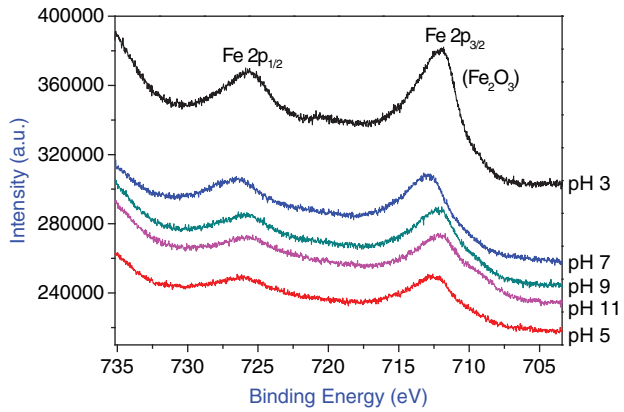

Fig. 7. Expanded Fe 2p3 spectra of $LiAl_5O_8:Fe^{3+}$ nanoparticles synthesized at various pH values. All the samples were annealed at 1200 °C for 6 h in air.

filled, the total orbital quantum number L = 0, spin quantum number S = 5/2. Thus the ground state term is ^6S. During the formation of Fe^{3+} ion, two electrons from 4*s* and one electron from 3d shell get released. The ground state electron gets excited at a wavelength of 453 nm from ^6S level to ^2I ($^2A_{2g}$) level. The excited electron from ^2I ($^2A_{2g}$) level relaxes to $^4T_{2g}$ level and de-excites or jumps to ^6S ground state level with an emission of 675 nm wavelength. Thus the high energy wavelength was down-converted to lower energy wavelength in the red region.

When Fe^{3+} doped $LiAl_5O_8$ is excited with UV light ($\lambda_{exc} = 453$ nm), electrons from $^6A_1$ (^6S) level get excited to reach ^4E ($^4A_1$) level. The excited electrons then reach to $^4T_1$ (^4G) level through successive relaxation steps and finally emits at 675 nm through transition between $^4T_1$ (^4G) → $^6A^1$ (^6S). In our case $LiAl_5O_8:Fe^{3+}$ nanophosphors display an absorption band near 453 nm and a relatively lower energy emission band around 675 nm. These wavelength converting phosphors are of high demand for preparing greenhouse films, which convert higher energy light to visible or near infra-red range.

Figure 9 shows the room temperature PL emission spectra of the $LiAl_5O_8:Fe^{3+}$ nanostructures synthesized at different pH values. The excitation of Fe^{3+} occurs at 453 nm (excitation wavelength) due to transitions $^6A_{1g} \rightarrow {}^2A_{2g}$, $^2T_{1g}$. Luminescence in $LiAl_5O_8:Fe^{3+}$ is attributed to the presence of Fe^{3+} in the octahedral site of $LiAl_5O_8$. In this ordered phase, each Li^+ ion is followed by three trivalent cations; octahedrally coordinated with oxygen.[32] The transition associated to Fe^{3+} in the octahedral position was also confirmed by ESR results where Fe^{3+} ions with 3d electronic configuration are seen to be preferentially occupied octahedral positions of the host lattice. The sample prepared at pH = 3 revealed emission peak at about 675.2 nm due to the $^4T_{2g}(^4G) \rightarrow {}^6A_1(^6S)$ transition of Fe^{3+} ions. The samples prepared at higher pH values revealed emission peaks at about 677.4, 676.8, 677.8 and 677.6 nm, for the pH values 5, 7, 9 and pH 11, respectively, which are slightly red-shifted in comparison with the emission from the sample prepared at pH = 3. The variation of emission intensity for the samples can be understood through the variation of activator concentration (Fe content) in them (see Table II). Variation of activator concentration was

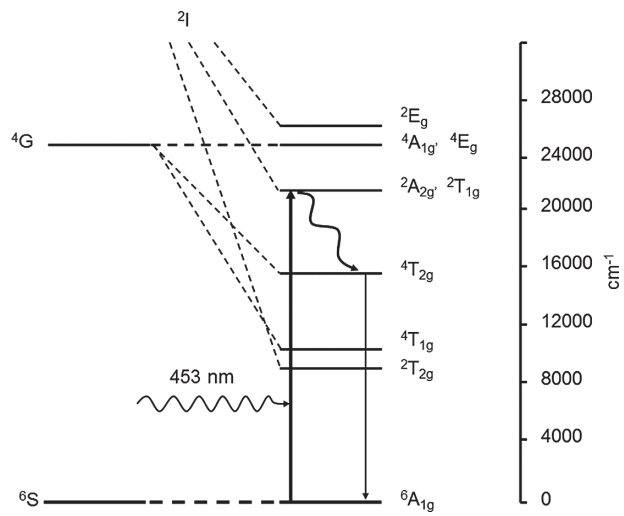

Fig. 8. Schematic presentation of the energy levels in $LiAl_5O_8:Fe^{3+}$ showing the down conversion of Fe^{3+} under 453 nm excitation.

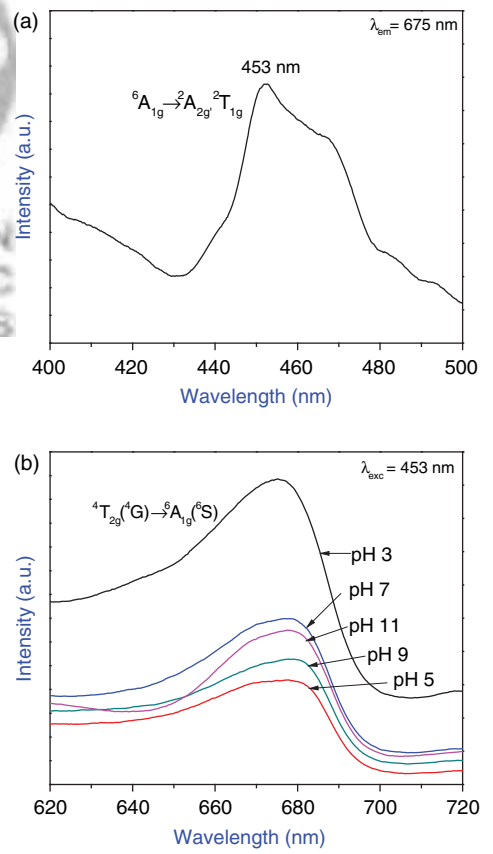

Fig. 9. Room temperature PL (a) excitation and (b) emission spectra of the $LiAl_5O_8:Fe^{3+}$ nanoparticles synthesized at different pH values. All the samples were annealed at 1200 °C for 6 h in air, and excited with the 453 nm emission of a xenon lamp.

reflected in luminescence spectra of $LiAl_5O_8:Fe^{3+}$ samples synthesized at different pH values.

4. CONCLUSION

Red emitting Fe^{3+} doped $LiAl_5O_8$ nanophosphors of well defined size and morphologies could be successfully synthesized in sol–gel process by varying the pH value of the reaction medium. The pH of the reaction medium plays important role in tailoring size and shape of the nanoparticles. The formation of $LiAl_5O_8:Fe^{3+}$ nanoparticles with varied morphology could be understood considering their bond formation process and pH value of the reaction medium. Emission intensity of the nanophosphors in red spectral region could be controlled by controlling the concentration of activator in them. Octahedral position of Fe^{3+} activator ions in the host lattice was found to be responsible for the red emissions of the nanophosphors. These wavelength converting nanophosphors have great potential for applications in energy conversion devices such as nanocomposite films used in green houses.

Acknowledgments: This work was financially supported by Korean Energy Technology Research and Development project, 2007–2010 and Engineering Research Center at Hanyang University through National Research Foundation.

References and Notes

1. W. K. Purves, D. Sadava, G. H. Orians, and H. C. Heller, Life, The Science of Biology, 7th edn., WHPS. W H Freeman and Company, NY (**2003**).
2. D. Jia and D. Hunter, *J. Wilhelm ECS Trans.* 6–27, 19 (**2008**).
3. M. Parker and H. Bothwick, *Plant Physiol.* 24, 345 (**1949**).
4. T. Justel, H. Bechtel, W. Mayr, and D. U. Wiechert, *J. Lumin.* 104, 137 (**2003**).
5. A. P. Jadhav, A. Pawar, C. W. Kim, H. G. Cha, U. Pal, and Y. S. Kang, *J. Phys. Chem. C* 113, 16652 (**2009**).
6. D. Jia, J. Zhu, B. Wu, and E. Shulin, *J. Lumin.* 93, 107 (**2001**).
7. L. Zuwu, L. Xi, and L. Jun, *Nat. Sci. J. Xiangton Univ.* 18, 49 (**1996**).
8. T. R. N. Kutty and N. Nayak, *J. Alloys. Compd.* 269, 75 (**1998**).
9. V. Singh, R. P. S. Chakradhar, J. Rao, and D. K. Kim, *Mater. Chem. Phys.* 110, 43 (**2008**).
10. D. Pan, D. Yuan, H. Sun, X. Xuan, C. Luan, S. Guo, Z. Li, and L. Wang, *Mater. Chem. Phys.* 96, 317 (**2006**).
11. V. Singh and T. K. Gundu Rao, *J. Solid State Chem.* 181, 1387 (**2008**).
12. V. Singh, V. Rai, I. Ledoux-Rak, and H. Y. Kwak, *Appl. Phys. B* 97–1, 103 (**2009**).
13. S. Hashimoto, K. Hattori, K. Inoue, A. Nakahashi, S. Honda, and Y. Iwamoto, *Mater. Res. Bull.* 44, 70 (**2009**).
14. M. M. C. Chou, C. C. Hsu, C. Y. Lee, and C. Chen, *Cryst. Growth Des.* 10–1, 191 (**2010**).
15. D. T. Palumbo, *J. Lumin.* 4, 89 (**1971**).
16. G. Pott and B. McNicol, *J. Chem. Phys.* 56, 5246 (**1972**).
17. Z. Liu, H. Wang, H. Li, and X. Wang, *Appl. Phys. Lett.* 72–15, 1823 (**1998**).
18. Z. L. Wang, Y. Liu, and Z. Zhang, Handbook of Nanophase and Nanostructured Materials, Kluwer Academic/Plenum Publishers, New York (**2002**), Vol. 1, p. 64.
19. P. Sharma, M. Jilavi, V. Varadan, and H. Schmidt, *J. Phys. Chem. Solids* 63, 171 (**2002**).
20. S. Sakka and K. Kamiya, *J. Non-Cryst. Solids* 48, 31 (**1982**).
21. P. Cagle, W. Klemperer, and C. Simmons, *Mater. Res. Soc. Symp. Proc.* 180, 29 (**1990**).
22. K. Keefer, *Adv. Chem. Ser., Am. Chem. Soc.* 224, 228 (**1990**).
23. L. Kelts, N. Effinger, and S. Melpoder, *J. Non-Cryst. Solids* 83, 353 (**1986**).
24. E. Pope and J. Mackenzie, *J. Non-Cryst. Solids* 87, 185 (**1986**).
25. W. G. Klemperer and S. D. Ramamurthi, *Mater. Res. Soc. Symp. Proc.* 121, 1 (**1988**).
26. C. Liu, H. Zhong, S. Komarnani, and C. Pantano, *J. Sol–Gel Sci. Tech.* 1, 141 (**1994**).
27. E. Boseman, D. Schoemaker, and C. R. Acad, *Sci. Paris* 1931 (**1961**).
28. R. Kedzie, D. Lyons, and M. Kestigian, *Phy. Rev.* 138, A918 (**1965**).
29. T. R. N. Kutty and N. Nayak, *Mater. Res. Bull.* 34–2, 249 (**1999**).
30. R. Cornell and U. Schwertmann, The Iron Oxides, Structures, Properties, Reactions, Occurrence and Uses, 2nd edn., Wiley–VCH, GmbH and Co. KGaA, Weinheim (**2003**), p. 347.
31. N. McIntyre and D. Zetaruk, *Anal. Chem.* 49, 1521 (**1977**).
32. N. Melamed, F. Barros, P. Viccaro, and J. Artman, *Phys. Rev. B* 5, 3377 (**1972**).